DOI 10.1007/s10946-023-10156-4
Journal of Russian Laser Research, Volume 44, Number 5, September, 2023

EXPLORING THE SURVIVAL AND SUDDEN DEATH OF QUANTUM CORRELATIONS IN AN OPEN ATOMIC LASER SYSTEM

Ebisa Mosisa Kanea[1*] and Chimdessa Gashu Feyisa[1,2,3]

[1] *Department of Physics, Jimma University*
P.O. Box 378, Jimma, Ethiopia

[2] *Institute of Atomic and Molecular Sciences, Academia Sinica*
Taipei 10617, Taiwan

[3] *Department of Physics, National Central University*
Taoyuan City 320317, Taiwan

Corresponding author e-mail: ebmosisa@gmail.com

Abstract

We focus our study on the quantum correlations of coupled photon pairs produced in an open atomic laser system, where quantum coherence is brought about by the superposition of a coherent atomic state and a coherent classical field. Quantum properties produced by photon–photon correlations are a long sought-after goal in quantum information science and technology, because photons combine at room temperature with high speed and long coherence times. The openness of the system under consideration allows quantum decoherence due to temperature and phase fluctuations to influence the quantum correlations generated. The competition between these quantum coherence and quantum decoherence leads to temporal quantum correlations, which we analyze using the time evolution of the density operator. Strong quantum correlations can be achieved by choosing an appropriate amplitude of the classical fields, treating temperature and phase fluctuations, and increasing the atomic injection rate over time. We also show that quantum entanglement is short-lived, quantum steering slowly decreases, but quantum discord increases with increasing heat bath temperature and atomic phase fluctuations. In this study, we explore the behavior of quantum correlations in an open atomic laser system and investigate the dynamics of entanglement, discord, and steering in this system and examine how they evolve over time.

Keywords: coherence, decoherence, photon pairs, quantum correlation.

1. Introduction

Quantum information and communication (QIC) began in the 20th century, when scientists developed quantum mechanics to explain physical phenomena that classical mechanics could not [1]. The field of quantum information theory is also an interdisciplinary field that overlaps with many fields, such as precision measurement, computer science, mathematics, information theory, engineering, materials science, and cryptography, among others. It is the result of applying the laws of quantum mechanics to govern the underlying information carrier for information processing tasks. Quantum uncertainty and quantum superposition are quantum mechanical principles that lie at the heart of quantum information

Manuscript submitted by the authors in English on September 11, 2023.

and communication applications [2]. Quantum uncertainty is not due to inaccurate measurement capability or loss/lack of information on the measurement processes, but is a fundamental feature inherent in nature itself between complementary quantum observables [3]. In addition, quantum superposition, often referred to as quantum coherence of two states, plays a fundamental role in quantum information and communication protocols. Quantum coherence is a nonlocal and nonclassical correlation of two or more quantum states [3–5]. It is responsible for quantum features, such as quantum discord, quantum entanglement, and quantum steering. These quantum correlations are the basis for quantum information and communication applications [6]. That is, the realization of QIC depends on methods to induce, quantify, and maintain the strength of quantum correlations captured in them.

In some circumstances, the presence of one quantum feature in a quantum system may indicate the presence or absence of additional quantum features in that system. For instance, quantum discord does not always require quantum entanglement to measure the strength of quantum correlations [7, 8]. Therefore, it is indeed highly interesting to study and compare these quantum features in an open quantum system that interacts with its environment. Quantum features generated from strongly coupled photon pairs have proven useful, powerful and suitable for QIC, in view of the fact that photons combine with high speed and long coherence times at room temperature [9, 10]. To this end, constructing a scheme that would produce strongly coupled photon pairs has become a major topic among current QIC research [11–18]. Ofer Kfir has explored photon coupling phenomena that unified strong coupling predictions with known electron–photon interactions to harness electron beams for quantum communication [13]. Researchers have explored photon coupling in the light driven and emitted by two highly interacting two-level emitters [14]. The study showed that frequency-dependent strong photon correlations can occur for QIC applications. In addition, a strongly correlated photon transport is observed in waveguides operating in the weak coupling region [15]. These photon correlations arise through an interplay of nonlinearity and coupling to a loss reservoir that creates a strong effective interaction between transmitted photons. Numerous theoretical and experimental investigations with two-photon atomic lasers [16], optical parametric oscillators [17], and parametric down converters [18] were also carried out.

Existing innovations have achieved remarkable control of quantum features generated by coupled photons. Much emphasis should also be given to the role of quantum decoherence, since quantum systems can perfectly maintain quantum coherence if they are completely isolated. This requirement is only ideal and is one of the daunting challenges in building perfectly isolated quantum devices, since loss of quantum coherence can occur through interaction with external environments. The phase fluctuation is also another source of coherence loss that should be closely controlled, even if not avoided. Therefore, generating and maintaining strong quantum coherence between quantum particles is one of the central goals of quantum information and communication protocols [19, 20]. To this end, atomic lasers have recently been shown to be active quantum systems with invaluable applications in quantum information processing [21].

In this work, we consider quantum coherence evolving between pairs of photons in an open atomic laser system. A coherent inducing classical field and a coherent superposition of atomic states are used to generate quantum coherence in the system. The atomic phase fluctuations and heat bath temperatures can also generate quantum decoherence in a quantum system. By adjusting the appropriate system parameters, such as the mean excitation of the heat bath, the atomic phase fluctuations, the number of atoms per unit time, and the classical field, we evaluate the quantum properties, using the standard master equation approach. This study provides valuable insight into the delicate nature of quantum correlations in an open atomic laser system. Understanding the dynamics and sudden death of these correlations is

critical for developing strategies to effectively preserve and manipulate quantum information. Moreover, in this paper, we contribute to the broader field of quantum information science, paving the way for future investigations into quantum correlations in complex open systems.

2. Model and Hamiltonian of the System

The quantum Hamiltonian terms describing the interaction of the atomic laser system with electromagnetic fields are derived using the rotating wave and electric dipole approximation. The total Hamiltonian in the interaction picture reads [22, 23]

$$\hat{H} = \sum_{m=1,2,3} \omega_m |m\rangle\langle m| + \omega_{21}\hat{o}_1^\dagger \hat{o}_1 + \omega_{32}\hat{o}_2^\dagger \hat{o}_2 + \hat{H}_I. \tag{1}$$

Here, the first term is atomic energy level with frequecies ω_1, ω_2, and ω_3, the second and third terms are photon energies with the annihilation operators $\hat{o}_1$ and $\hat{o}_2$ and resonance frequencies $\omega_{21} = \omega_2 - \omega_1$ and $\omega_{32} = \omega_3 - \omega_2$, and the last term $\hat{H}_I$ is the interaction Hamiltonian between the atoms and cavity photons and classical field. The interaction Hamiltonian can be obtained using the unitary operator $\hat{U} = exp(-i\hat{H}_0 t)$, where $\hat{H}_0 = \sum_{m=1,2,3} \omega_m |m\rangle\langle m| + \omega_{21}\hat{o}_1^\dagger \hat{o}_1 + \omega_{32}\hat{o}_2^\dagger \hat{o}_2$; it is [23, 24]

$$\hat{H}_I = ig\left[\hat{o}_1^\dagger |2\rangle\langle 1| + \hat{o}_2^\dagger |3\rangle\langle 2| - |1\rangle\langle 2|\hat{o}_1 - |2\rangle\langle 3|\hat{o}_2] + i\frac{\xi}{2}[|3\rangle\langle 1| - |1\rangle\langle 3|\right], \tag{2}$$

where g is the coupling constant between the atom and cavity mode; it is assumed the same for both transitions, and ξ defines the amplitude of the classical field that couples the top and bottom states of the atoms in the cavity. It should be resonant with the frequency $\omega = \omega_{32} + \omega_{21}$; see Fig. 1.

We are interested to consider an atom, which is initially in a state

$$|\psi(0)\rangle = C_1(0)|1\rangle + e^{-i\phi}C_3(0)|3\rangle, \tag{3}$$

where ϕ is an arbitrary phase difference between the two states. It is reasonable to assume that ϕ is the sum of a mean value ϕ_0 and a small deviation $\delta\phi$, $\phi = \phi_0 + \delta\phi$. The arbitrary phase difference can also be considered as a Gaussian random process with a phase dispersion $\delta\phi = 0$ and a phase fluctuation $\frac{\delta\phi^2}{2} = \theta$ [24, 25]. Therefore, θ is generally designated simply as a phase fluctuation. Taking into account

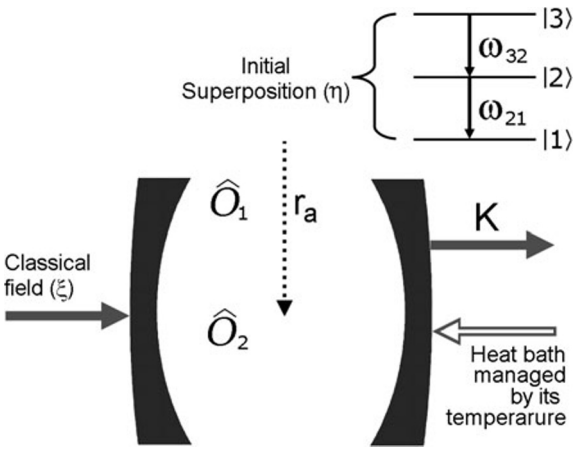

Fig. 1. Schematic representation of an atomic laser system coupled to a reservoir. Here, r_a is the number of atoms per unit time introduced into the cavity, where κ is the photon attenuation rate. It is clearly indicated that the atomic energy states are represented by $|3\rangle$, $|2\rangle$, and $|1\rangle$. The photon modes $\hat{o}_1$ and $\hat{o}_2$ are resonant to the atomic state dipole transitions coming from $|3\rangle \to |2\rangle$ and $|2\rangle \to |1\rangle$. However, they are off-resonant to the dipole-forbidden transitions from $|3\rangle$ to $|1\rangle$, and vice versa. The cavity radiation modes are at resonance with the transition $|3\rangle \to |2\rangle$ and $|2\rangle \to |1\rangle$ having frequencies $\omega = \omega_{32} + \omega_{21}$.

the phase fluctuation, the initial density operator for a single atom can now be expressible in the following form:

$$\rho(0) = \rho_{11}^{(0)}|1\rangle\langle 1| + \rho_{13}^{(0)}e^{-\theta}|1\rangle\langle 3| + \rho_{31}^{(0)}e^{-\theta}|3\rangle\langle 1| + \rho_{33}^{(0)}|3\rangle\langle 3|, \tag{4}$$

where $\rho_{11}^{(0)} = |C_1(0)|^2$ and $\rho_{33}^{(0)} = |C_3(0)|^2$ are the probability for the atom to be in states $|1\rangle$ and $|3\rangle$, and $\rho_{13}^{(0)} = C_1(0)C_3^*(0)$ and $\rho_{31}^{(0)} = C_3(0)C_1^*(0)$ represent the atomic state superposition at the initial time. We also note that $|\rho_{13}^{(0)}|^2 = |\rho_{31}^{(0)}|^2 = \rho_{11}^{(0)}\rho_{33}^{(0)}$.

Employing the linear and adiabatic approximation schemes in the good cavity limit, we can find the evolution equation of the density operator for the cavity modes. The full descriptions of the evolution of the coupled atom–radiation system can be found in [16]. The cavity states, with the initial vacuum state, are calculated after tracing out the atomic variables; they are

$$\begin{aligned}\frac{d}{dt}\hat{\rho}(t) = \quad & \frac{AI}{2H}\left[2\hat{o}_1^\dagger\hat{\rho}\hat{o}_1 - \hat{\rho}\hat{o}_1\hat{o}_1^\dagger - \hat{o}_1\hat{o}_1^\dagger\hat{\rho}\right] + \frac{AJ}{2H}\left[(2\hat{o}_2\hat{\rho}\hat{o}_2^\dagger - \hat{\rho}\hat{o}_2^\dagger\hat{o}_2 - \hat{o}_2^\dagger\hat{o}_2\hat{\rho}\right] \\ & + \frac{AK}{2H}\left[\hat{o}_1^\dagger\hat{\rho}\hat{o}_1^\dagger - \hat{\rho}\hat{o}_2^\dagger\hat{o}_1^\dagger + \hat{o}_2\hat{\rho}\hat{o}_1 - \hat{o}_1\hat{\rho}\hat{o}_2\right] + \frac{AL}{2H}\left[\hat{o}_1^\dagger\hat{\rho}\hat{o}_2^\dagger - \hat{o}_2^\dagger\hat{o}_1^\dagger\hat{\rho} + \hat{o}_2\hat{\rho}\hat{o}_1 - \hat{\rho}\hat{o}_1\hat{o}_2\right], \end{aligned} \tag{5}$$

where we use $\rho = \rho(t)$ for simplicity. In the above equation, $A = \dfrac{2g^2 r_a}{\gamma^2}$ is an effective number of atoms per unit time, and γ is the spontaneous decay rate, which is taken to be the same for both transitions. The rest parameters are functions of the atomic coherence and populations given by

$$H = (1 + (\xi/\gamma)^2)\left[1 + \frac{(\xi/\gamma)^2}{4}\right], \qquad I = \rho_{11}^{(0)}\left[1 + \frac{(\xi/\gamma)^2}{4}\right] - \rho_{13}^{(0)}\frac{3\xi/\gamma}{2} + \rho_{33}^{(0)}\frac{3(\xi/\gamma)^2}{4},$$

$$J = \rho_{11}^{(0)}\frac{3}{4}(\xi/\gamma)^2 + \rho_{13}^{(0)}\frac{3\xi/\gamma}{2} + \rho_{33}^{(0)}\left[1 + \frac{(\xi/\gamma)^2}{4}\right],$$

$$K = -\rho_{11}^{(0)}\frac{\xi/\gamma}{2}\left[1 - \frac{(\xi/\gamma)^2}{2}\right] - \rho_{13}^{(0)}\left[1 - \frac{(\xi/\gamma)^2}{2}\right] + \rho_{33}^{(0)}\xi/\gamma\left[1 + \frac{(\xi/\gamma)^2}{4}\right],$$

$$\text{and} \qquad L = -\rho_{11}^{(0)}\frac{\xi}{\gamma}\left[1 + \frac{(\xi/\gamma)^2}{4}\right] - \rho_{13}^{(0)}\left[1 - \frac{(\xi/\gamma)^2}{2}\right] + \rho_{33}^{(0)}\frac{\xi/\gamma}{2}\left[1 - \frac{(\xi/\gamma)^2}{2}\right].$$

We note that Eq. (5) along with the coefficients Eqs. (6)–(8) represent the cavity state without the effect of an external environment. When the effect of thermal environment is included, the time evolution of the density operator for the two-mode photons coupled to a two-mode heat bath becomes [26]

$$\begin{aligned}\frac{d\hat{\rho}}{dt} = \quad & \frac{\kappa}{2}(\bar{N}_{\rm th}+1)\left[2\hat{o}_1\hat{\rho}\hat{o}_1^\dagger - \hat{o}_1^\dagger\hat{o}_1\hat{\rho} - \hat{\rho}\hat{o}_1^\dagger\hat{o}_1\right] + \frac{1}{2}\kappa\bar{N}_{\rm th}\left[2\hat{o}_2^\dagger\hat{\rho}\hat{o}_2 - \hat{o}_2\hat{o}_2^\dagger\rho - \hat{\rho}\hat{o}_2\hat{o}_2^\dagger\right] \\ & + \frac{1}{2}\left[\frac{AI}{H} + \kappa\bar{N}_{\rm th}\right]\left[2\hat{o}_1^\dagger\hat{\rho}\hat{o}_1 - \hat{o}_1\hat{o}_1^\dagger\hat{\rho} - \hat{\rho}\hat{o}_1\hat{o}_1^\dagger\right] + \frac{1}{2}\left(\frac{AJ}{H} + \kappa(\bar{N}_{\rm th}+1)\right)\left[2\hat{o}_2\hat{\rho}\hat{o}_2^\dagger - \hat{o}_2^\dagger\hat{o}_2\hat{\rho} - \hat{\rho}\hat{o}_2^\dagger\hat{o}_2\right] \\ & - \frac{AK}{2H}\left[\hat{o}_1\hat{o}_2\hat{\rho} - \hat{o}_1^\dagger\hat{\rho}\hat{o}_2^\dagger + \hat{\rho}\hat{o}_2^\dagger\hat{o}_1^\dagger - \hat{o}_2\hat{\rho}\hat{o}_1\right] - \frac{AL}{2H}\left[\hat{o}_2^\dagger\hat{o}_1^\dagger\hat{\rho} - \hat{o}_1^\dagger\hat{\rho}\hat{o}_2^\dagger + \hat{\rho}\hat{o}_1\hat{o}_2 - \hat{o}_2\hat{\rho}\hat{o}_1\right]. \end{aligned} \tag{6}$$

We use Eq. (6) to study the dynamics of the quantum system. The gain of the cavity light for mode $\hat{o}_1$ and the loss for mode $\hat{o}_2$ are considered in terms proportional to I and J, respectively. Quantum coherence is built up in the system due to the presence of the terms proportional to K and L. In view

of Eq. (6), we can obtain the time evolution of photon annihilation operators; they are

$$\frac{d}{dt}\hat{o}_1(t) = -\frac{\mu_1}{2}\hat{o}_1(t) + \frac{\nu_1}{2}\hat{o}_2^{\dagger}(t) + \hat{o}_1^{(\mathrm{in})}(t), \tag{7}$$

$$\frac{d}{dt}\hat{o}_2^{\dagger}(t) = -\frac{\mu_2}{2}\hat{o}_2^{\dagger}(t) - \frac{\nu_2}{2}\hat{o}_1(t) + (\hat{o}_2^{(\mathrm{in})})^*(t), \tag{8}$$

where $\mu_1 = \kappa - AI/H$, $\mu_2 = \kappa - AI/H$, $\nu_1 = AK/H$, $\nu_2 = AL/H$ and $\hat{o}_1^{(\mathrm{in})}(t)$, and $(\hat{o}_2^{(\mathrm{in})})^*(t)$ are reservoir input noise operators. With the help of Eqs. (7) and (8), the relevant expectation values of these operators become

$$\langle \hat{o}_1^{(\mathrm{in})}(t)\rangle = \langle o_1(t)\hat{o}_1^{(\mathrm{in})}(t)\rangle = 0, \tag{9}$$

$$\langle \hat{o}_2^{(\mathrm{in})}(t)\hat{o}_2^{(\mathrm{in})}(t')\rangle = \langle (\hat{o}_1^{(\mathrm{in})})^*(t)\hat{o}_2^{(\mathrm{in})}(t')\rangle = 0, \tag{10}$$

$$\langle o_1^*(t)\hat{o}_1^{(\mathrm{in})}(t)\rangle + \langle o_1(t)(\hat{o}_1^{(\mathrm{in})})^*(t)\rangle = \frac{AI}{H} + \kappa\bar{N}_{\mathrm{th}}, \tag{11}$$

$$\langle o_2^*(t)\hat{o}_2^{(\mathrm{in})}(t)\rangle + \langle o_2(t)(\hat{o}_2^{(\mathrm{in})})^*(t)\rangle = \kappa\bar{N}_{\mathrm{th}}, \tag{12}$$

$$\langle o_2(t)\hat{o}_1^{(\mathrm{in})}(t)\rangle + \langle o_1(t)\hat{o}_2^{(\mathrm{in})}(t)\rangle = -\frac{AL}{H}. \tag{13}$$

Using these correlation properties of noise operators, we get the full expressions of the cavity mode operators at any time t.

To do so, first we have to specify the initial atomic states prior to their injection into the laser cavity. In Eq. (4), one can see that the probabilities of atoms to be found in the states $|1\rangle$ and $|3\rangle$ can be related to each other through a new parameter defined by $\eta = \rho_{11}^0 - \rho_{33}^0$. From the fact that the sum of these probabilities is equal to one, we can obtain $\rho_{11}^0 = \dfrac{1+\eta}{2}$, $\rho_{33}^0 = \dfrac{1-\eta}{2}$, and thus $\rho_{13}^0 = \rho_{31}^0 = \dfrac{1}{2}\sqrt{1-\eta^2}$. The minimum and maximum of parameter η correspond to $\rho_{33}^0 = 1$ and $\rho_{11}^0 = 1$, respectively. In this case, there is no quantum coherence induced by atomic state superposition, but coherence induced via a classical field still exists. Here, the eligible η values lie in between $-1 \le \eta \le 1$, which is the case of lasing without the population inversion. This amounts to fixing the probability amplitudes to $0 \le \rho_{11}^0 \le 50\%$ and $50\% \le \rho_{33}^0 \le 100\%$. Now we rewrite Eqs. (7) and (8), using Eqs. (9)–(13), as follows:

$$\frac{d}{dt}\hat{o}_1(t) = -\xi_+\hat{o}_1(t) - \eta_+\hat{o}_2^{\dagger}(t) + \hat{o}_1^{(\mathrm{in})}(t), \tag{14}$$

$$\frac{d}{dt}\hat{o}_2^{\dagger}(t) = -\xi_-\hat{o}_2^{\dagger}(t) - \eta_-\hat{o}_1(t) + (\hat{o}_2^{(\mathrm{in})})^*(t), \tag{15}$$

in which $\xi_+ = \dfrac{1}{2}\left(\kappa - \dfrac{AI}{H}\right)$, $\xi_- = \dfrac{1}{2}\left(\kappa + \dfrac{AJ}{H}\right)$, $\eta_+ = -\dfrac{1}{2}\dfrac{AK}{H}$, and $\eta_- = \dfrac{1}{2}\dfrac{AL}{H}$.

The solutions of coupled differential equations (14), (15), with the help of correlation properties of noise operators Eqs. (9)–(13), can be written as

$$\hat{o}_1(t+\tau) = A_+(\tau)\hat{o}_1(t) + B_+(\tau)\hat{o}_2^{\dagger}(t) + F_+(t+\tau) + W_+(t+\tau), \tag{16}$$

$$\hat{o}_2(t+\tau) = A_-(\tau)\hat{o}_2(t) + B_-(\tau)\hat{o}_1^{\dagger}(t) + F_-(t+\tau) + W_-(t+\tau), \tag{17}$$

where

$$A_{\pm}(\tau) = \frac{1}{2}\left[(1 \pm p)e^{-\lambda_- \tau} + (1 \mp p)e^{-\lambda_+ \tau}\right], \tag{18}$$

$$B_{\pm}(\tau) = \frac{q_{\pm}}{2}\left[e^{-\lambda_+ \tau} - e^{-\lambda_- \tau}\right], \tag{19}$$

$$F_+(t+\tau) = \frac{1}{2}\int_0^\tau \left[(1+p)e^{-\lambda_-(\tau-\tau')} + (1-p)e^{-\lambda_+(\tau-\tau')}\right]\hat{o}_1^{(in)}(t+\tau')\,d\tau', \tag{20}$$

$$F_-(t+\tau) = \frac{1}{2}\int_0^\tau \left[(1-p)e^{-\lambda_-(\tau-\tau')} + (1+p)e^{-\lambda_+(\tau-\tau')}\right]\hat{o}_2^{(in)}(t+\tau')\,d\tau', \tag{21}$$

$$W_+(t+\tau) = \frac{q_+}{2}\int_0^\tau \left[e^{-\lambda_+(\tau-\tau')} - e^{-\lambda_-(\tau-\tau')}\right](\hat{o}_2^{(in)})^*(t+\tau')\,d\tau', \tag{22}$$

$$W_-(t+\tau) = \frac{q_-}{2}\int_0^\tau \left[e^{-\lambda_+(\tau-\tau')} - e^{-\lambda_-(\tau-\tau')}\right](\hat{o}_1^{(in)})^*(t+\tau')\,d\tau', \tag{23}$$

in which

$$p = \frac{(\xi_- - \xi_+)}{\sqrt{(\xi_+ - \xi_-)^2 + 4\eta_+\eta_-}}, \tag{24}$$

$$q_{\pm} = \frac{\eta_{\pm}}{\sqrt{(\xi_+ - \xi_-)^2 + 4\eta_+\eta_-}}. \tag{25}$$

$$\lambda_+ = \frac{1}{2}\left[(\xi_+ + \xi_-) + \sqrt{(\xi_+ - \xi_-)^2 + 4\eta_+\eta_-}\right], \tag{26}$$

$$\lambda_- = \frac{1}{2}\left[(\xi_+ + \xi_-) - \sqrt{(\xi_+ - \xi_-)^2 + 4\eta_+\eta_-}\right]. \tag{27}$$

Our calculations entirely depend on Eqs. (16) and (17) and the associated coefficients. For instance, the mean photon numbers of mode 1 and mode 2 are given by $n_1(t) = \langle \hat{o}_1^\dagger(t)\hat{o}_1(t)\rangle$ and $n_2(t) = \langle \hat{o}_2^\dagger(t)\hat{o}_2(t)\rangle$, while $n_{12}(t) = \langle \hat{o}(t)\hat{o}_2(t)\rangle$ is the mean number of the cross correlation of the two modes. We solve them, usubg Eqs. (16) and (17). Moreover, the mean photon numbers $n_1(t)$, $n_2(t)$, and $n_{12}(t)$ are very important for the analysis of quantum correlations given in the next sections.

3. Quantum Correlations

3.1. Quantum Steering

Quantum steering has become of great research interest due to its asymmetric nature and device independent behavior. A Gaussian state, $\hat{\rho} = \rho(\hat{o}_1, \hat{o}_2)$ for two-mode photons can be described by a symplectic matrix. whose elements are given by [8, 27]

$$G_{ij} = \frac{1}{2}\langle \hat{x}_i\hat{x}_j + \hat{x}_j\hat{x}_i\rangle - \langle \hat{x}_i\rangle\langle \hat{x}_j\rangle, \tag{28}$$

in which $i, j = 1, 2, 3, 4$. The quadrature operators are defined as $\hat{x}_1 = \hat{o}_1 + \hat{o}_1^\dagger$, $\hat{x}_2 = i(\hat{o}_1^\dagger - \hat{o}_1)$, $\hat{x}_3 = \hat{o}_2 + \hat{o}_2^\dagger$, and $\hat{x}_4 = i(\hat{o}_2^\dagger - \hat{o}_2)$. In view of these definitions, the only non-vanishing terms in the

extended covariance matrix are

$$G = \begin{pmatrix} G_1 & G_{12} \\ G_{12}^T & G_2 \end{pmatrix} = \begin{pmatrix} m_{11}(t) & 0 & m_{13}(t) & 0 \\ 0 & m_{22}(t) & 0 & m_{24}(t) \\ m_{13}^*(t) & 0 & m_{33}(t) & 0 \\ 0 & m_{24}^*(t) & 0 & m_{44}(t) \end{pmatrix}, \tag{29}$$

where $m_{11}(t) = m_{22}(t) = \sqrt{\det(G_1)} = 2n_1(t) + 1$, $m_{33}(t) = m_{44}(t) = \sqrt{\det(G_2)} = 2n_2(t) + 1$, and the real off-diagonal entries are $m_{13}(t) = -m_{24}(t) = \sqrt{-\det(G_{12})} = 2n_{12}(t)$. Here, $n_1(t)$ and $n_2(t)$ represent the mean photon numbers of mode 1 and mode 2, while $n_{12}(t)$ is the mean number of the cross correlation of the two modes defined in the previous section. Note that all matrix elements of Eq. (29) are real; hence, one can easily observe that it is a symplectic matrix. This is a sound argument supporting the Gaussian character of the two-mode electromagnetic state.

One can also easily verify that

$$\det(G) = [m_{11}(t)m_{33}(t) + m_{13}(t)m_{24}(t)]^2 . \tag{30}$$

On the other hand, the corresponding symplectic eigenvalues of the covariance matrix described in Eq. (29) are given by

$$s_{\pm} = \sqrt{\frac{a \pm \sqrt{a^2 - 4\det(G)}}{2}}, \tag{31}$$

where $a = \det(G_1) + \det(G_2) + 2\det(G_{12})$, and $s_{\pm}$ are invariant quantities.

According to the formulations of Gaussian quantum steering [27], the necessary and sufficient condition for two-mode Gaussian quantum steerability from $\hat{o}_1 \to \hat{o}_2$ is

$$S^{\hat{o}_1 \to \hat{o}_2} = \Delta x_{3|1} \Delta x_{4|2} < 1, \tag{32}$$

where the conditional variances are defined by $[\Delta x_{3|1}]^2 = [\Delta(x_3 - g_x x_1)]^2$ and $[\Delta x_{4|2}]^2 = [\Delta(x_4 + g_p x_2)]^2$, with g_x and g_p being optimization factors, which are real constants adjustable to minimize quantum fluctuations of the quadrature operators [27, 28], from which one can obtain

$$S^{\hat{o}_1 \to \hat{o}_2} = \sqrt{\left[m_{11}(t) - \frac{m_{13}^2(t)}{m_{33}(t)}\right]\left[m_{11}(t) - \frac{m_{24}^2(t)}{m_{33}(t)}\right]}, \tag{33}$$

where $g_x = \dfrac{m_{13}(t)}{m_{33}(t)}$ and $g_p = -\dfrac{m_{24}(t)}{m_{33}(t)}$ [28].

One could also easily swap the roles of G_1 and G_2 to obtain the measurement of Gaussian quantum steering $S^{\hat{o}_2 \to \hat{o}_1}$. Quantum steering is exhibited in the quantum system when either or both $S^{\hat{o}_1 \to \hat{o}_2}$ and $S^{\hat{o}_2 \to \hat{o}_1}$ are smaller than unity.

In order to investigate $S^{\hat{o}_1 \to \hat{o}_2}$ and $S^{\hat{o}_2 \to \hat{o}_1}$, we plot $S^{\hat{o}_1 \to \hat{o}_2}$ and $S^{\hat{o}_2 \to \hat{o}_1}$ versus the dimensionless parameter γt by varying the relevant system parameters. An in-depth analysis of quantum steering and its comparison with other quantum features can be made using 2D plots as follows below.

In Figs. 2 and 3 a, we plot the Gaussian quantum steering between the light modes $\hat{o}_1$ and $\hat{o}_2$ against the dimension parameter γt and quantum coherence $\dfrac{\xi}{\gamma}$. According to [27], the steerability from mode $\hat{o}_1$

to mode $\hat{o}_2$ is strong, when the quantum noise is minimized. However, there is no quantum steering if $S^{\hat{o}_1\to\hat{o}_2} \geq 1$. In this regard, we show that initially there is no quantum steering between light modes, at which time $S^{\hat{o}_1\to\hat{o}_2} = 1$. With increasing dimensionless parameter γt, the quantum steering between the two light modes is strengthened. This means that quantum coherence provides sufficient time to generate steerable quantum correlations between the light modes, as can be seen below.

In Figs. 2–4, we plot quantum steering $S^{\hat{o}_1\to\hat{o}_2}$ versus the dimensionless parameter γt by varying parameters of atomic injection with time, heat bath, and phase fluctuation.

Quantum steering from mode $\hat{o}_1$ to mode $\hat{o}_2$ becomes weaker with increasing quantum decoherence, while it becomes stronger with increasing atomic injection rate. We observe that the quantum steering of $\hat{o}_1 \to \hat{o}_2$ increases rapidly over time until it reaches a peak value that remains under thermal decoherence for a long period of time, but decreases slightly over time under phase fluctuations. This is pretty unlike the behavior of quantum entanglement, whose peak strength is short-lived and suffers sudden death in the long time scale. That is, quantum steering is stronger than entanglement under the influence of quantum decoherence.

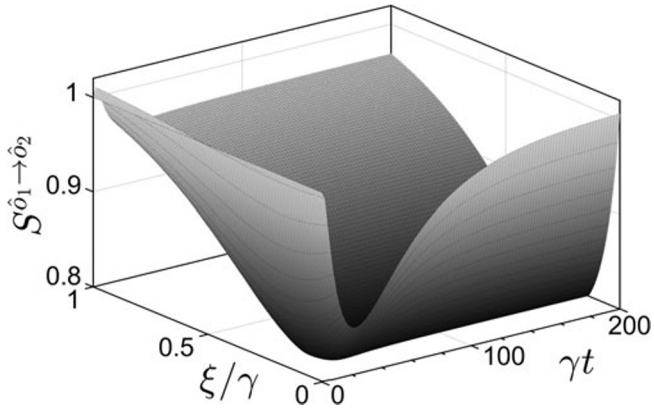

Fig. 2. Time evolution of quantum steering $S^{\hat{o}_1\to\hat{o}_2}$ against the dimensionless parameter γt and ξ/γ for $r_a = 10$ kHz, $\kappa = 0.5$ kHz, $g = 0.8\gamma$, $\theta = 0.00$, $\eta = 0.1$ and $\bar{N}_{\rm th} = 0.5$.

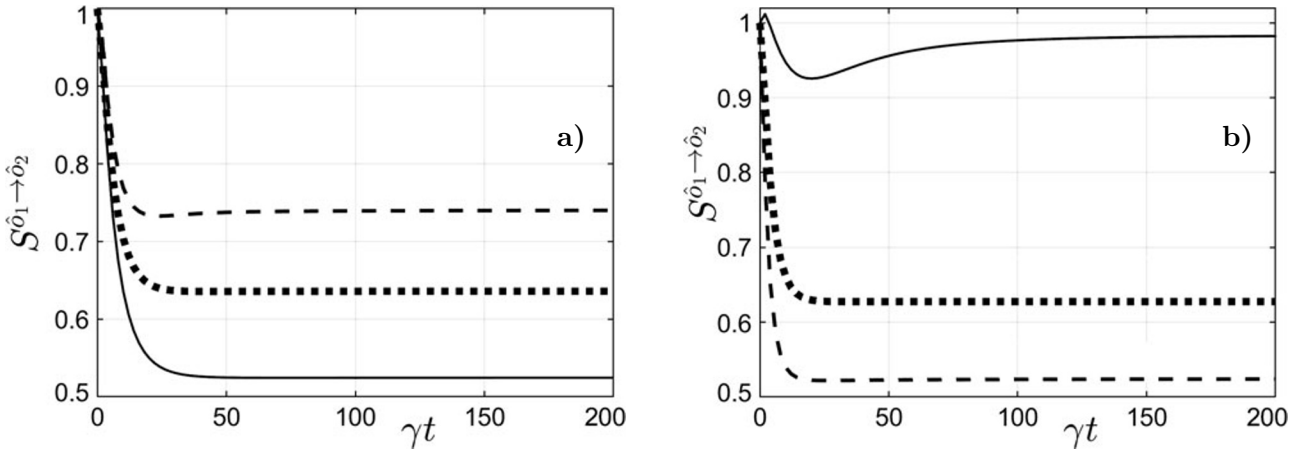

Fig. 3. Time evolution of quantum steering $S^{\hat{o}_1\to\hat{o}_2}$ against the dimensionless parameter γt for $r_a = 5$ kHz, $\kappa = 0.5$ kHz, $\eta = 0.1$, $g = 0.8\gamma$, $\xi = 0.1\gamma$, $\theta = 0.01$, and different value of $\bar{N}_{\rm th} = 0.00$ (the solid curve), 0.25 (the dotted curve), and 0.50 (the dashed curve) (a) and $\bar{N}_{\rm th} = 0.50$, $\kappa = 0.5$ kHz, $\eta = 0.1$, $g = 0.8\gamma$, $\xi = 0.1\gamma$, $\theta = 0.01$, $r_a = 5$ (the solid curve), 15 (the dotted curve), and 25 kHz (the dashed curve) (b).

3.2. Quantum Entanglement

In this section, we investigate quantum entanglement of the coupled photon pairs. In general, a pair of quantum-mechanical particles is in entangled state if and only if their individual states cannot be

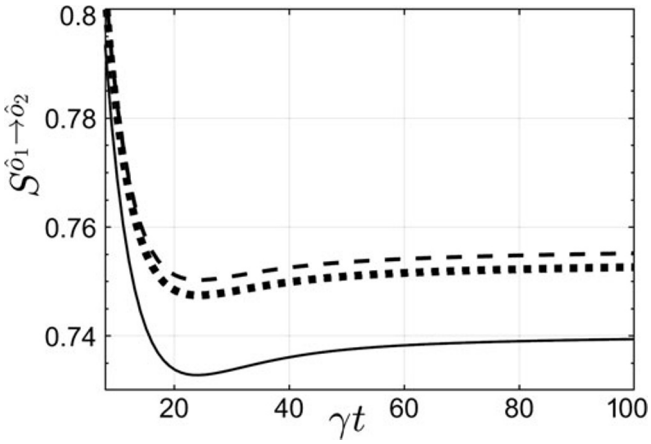

Fig. 4. Time evolution of quantum steering $S^{\hat{o}_1\to\hat{o}_2}$ against the dimensionless parameter γt for $\bar{N}_{\rm th} = 0.1$, $\kappa = 0.5$ kHz, $\xi = 0.1\gamma$, $\eta = 0.1$, $g = 0.8\gamma$, $r_a = 2$ kHz, and different value of $\theta = 0.00$ (the solid curve), 0.0125 (the dotted curve), and 0.015 (the dashed curve).

expressed as a product of the states of its separate constituents [5]. Thus, we can write

$$\hat{\rho} \neq \sum_i P_i \hat{\rho}_i^{(1)} \otimes \hat{\rho}_i^{(2)}, \tag{34}$$

where $P_i \geq 0$ and $\sum_i P_i = 1$ represents the normalization condition for the combined density state of the composite system.

Though numerous criteria of entanglement measures have been developed and currently available in the literature, here we apply the criterion set by Duan et al. [29]. This criterion is highly interesting due to its direct utilization to quantify quantum squeezing.

Based on this criterion, a quantum state of the system is entangled if the sum of the variances of the EPR-type operators $\hat{x}$ and $\hat{p}$ satisfies the condition

$$\frac{\Delta x^2 + \Delta p^2}{2} < 1, \tag{35}$$

in which $\hat{x} = \hat{x}_a - \hat{x}_b$, and $\hat{p} = \hat{p}_a + \hat{p}_b$. Here, $\hat{x}_a = \frac{1}{\sqrt{2}}(\hat{o}_1^\dagger + \hat{o}_1)$, $\hat{x}_b = \frac{1}{\sqrt{2}}(\hat{o}_2^\dagger + \hat{o}_2)$ and $\hat{p}_a = \frac{i}{\sqrt{2}}(\hat{o}_1^\dagger - \hat{o}_1)$, $\hat{p}_b = \frac{i}{\sqrt{2}}(\hat{o}_2^\dagger - \hat{o}_2)$ are the quadrature operators of the cavity-mode photons.

We are now able to determine the variances of $\hat{x}$ and $\hat{p}$. As for the variance of $\hat{x}$, $\Delta x^2 = \langle x^2\rangle - \langle x\rangle^2$, the first term can be described as

$$\langle x^2\rangle = \frac{1}{2}\left[2 + 2\langle \hat{o}_1^\dagger \hat{o}_1\rangle + 2\langle \hat{o}_2^\dagger \hat{o}_2\rangle - \left(\langle \hat{o}_1 \hat{o}_2\rangle + \langle \hat{o}_1^\dagger \hat{o}_2^\dagger\rangle + \langle \hat{o}_2 \hat{o}_1\rangle + \langle \hat{o}_2^\dagger \hat{o}_1^\dagger\rangle\right)\right]. \tag{36}$$

It is not difficult to find the solution of Eq. (36), it reads

$$\langle x^2\rangle = \frac{1}{2}\left[2 + 2\langle \hat{o}_1^\dagger \hat{o}_1\rangle + 2\langle \hat{o}_2^\dagger \hat{o}_2\rangle - 4\langle \hat{o}_1 \hat{o}_2\rangle\right]. \tag{37}$$

Moreover, it is straightforward to see that

$$\langle x\rangle^2 = 0. \tag{38}$$

With the help of Eqs. (37) and (38), the variance of $\hat{x}$ becomes

$$\Delta x^2 = \langle x^2\rangle = 1 + \langle \hat{o}_1^\dagger \hat{o}_1\rangle + \langle \hat{o}_2^\dagger \hat{o}_2\rangle - 2\langle \hat{o}_1 \hat{o}_2\rangle. \tag{39}$$

Following the same procedure, it is possible to verify that

$$\Delta p^2 = 1 + \langle \hat{o}_1^\dagger \hat{o}_1 \rangle + \langle \hat{o}_2^\dagger \hat{o}_2 \rangle - 2\langle \hat{o}_1 \hat{o}_2 \rangle. \tag{40}$$

Thus, we find the sum of the variances of $\hat{x}$ and $\hat{p}$ as follows:

$$\frac{\Delta x^2 + \Delta p^2}{2} = 1 + n_1(t) + n_2(t) - 2n_{12}(t). \tag{41}$$

In order to investigate the entanglement of the two-mode radiation with this criterion, we plot $\frac{\Delta x^2 + \Delta p^2}{2}$ for the same system parameters as used in the previous section. The quantum system exhibits 100% entangled and is non-entangled, when the sum of fluctuations in the position-like and momentum-like operators reduces to zero, $\frac{\Delta x^2 + \Delta p^2}{2} = 0$, and greater than one, $\frac{\Delta x^2 + \Delta p^2}{2} > 1$, respectively.

The dependence of $\frac{\Delta x^2 + \Delta p^2}{2}$ on time, coherent classical field, and coherent superposition can be inferred from Figs. 5 and 6.

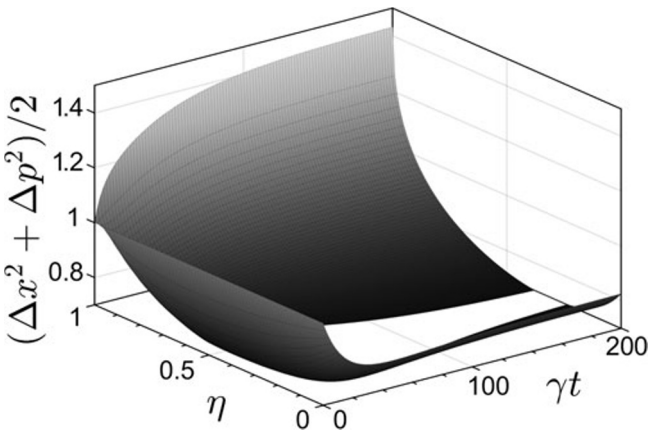

Fig. 5. Time evolution of quantum entanglement $\frac{\Delta x^2 + \Delta p^2}{2}$ against the dimensionless parameter γt and η of the photon pairs for $r_a = 10$ kHz, $\kappa = 0.5$ kHz, $g = 0.8\gamma$, $\xi = 0.1\gamma$, $\theta = 0.00$, and $\bar{N}_{\rm th} = 0.5$.

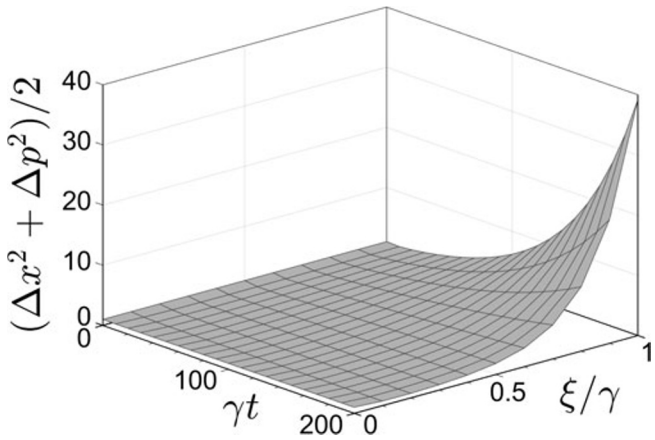

Fig. 6. Time evolution of quantum entanglement $\frac{\Delta x^2 + \Delta p^2}{2}$ against the dimensionless parameter γt and ξ/γ of the photon pairs for $r_a = 10$ kHz, $\kappa = 0.5$ kHz, $\eta = 0.1$, $g = 0.8\gamma$, $\theta = 0.00$, and $\bar{N}_{\rm th} = 0.5$.

Despite the presence of a large amount of the heat-bath parameters, the considered optical system demonstrates quite robust quantum entanglement according to Duan et al. [29] inseparability criterion mentioned in Table 1.

Table 1. Conditions for Entangled and Non-Entangled Light According to the Duan Criterion [23].

Entangled (100%)	Entangled (0 – 100%)	Non-Entangled (0%)
$\frac{\Delta x^2 + \Delta p^2}{2} = 1$	$1 < \frac{\Delta x^2 + \Delta p^2}{2} < 0$	$\frac{\Delta x^2 + \Delta p^2}{2} > 1$

We show that the quantum coherence resources the quantum entanglement, which highly varies with parameters describing the quantum coherence. Photon pairs are non-entangled in the absence of atomic state superposition even if the parameter of the coherent classical field is nonzero $\xi/\gamma > 0$. In other words, the classical field is efficiently used up to induce quantum coherence of non-classical features, when sufficient numbers of atoms are available in the excited energy state. Pumping electrons in atoms to the excited state would be an additional task for the classical field, when none of them are initially in the excited state. For example, photon pairs are non-entangled for $\eta = 1$, though a classical field of $\xi = \dfrac{\gamma}{10}$ is used to couple them; see Fig. 5. To get more insight on the roles of specific system parameters, we use 2D plots that are well suited to study dynamics of quantum entanglement.

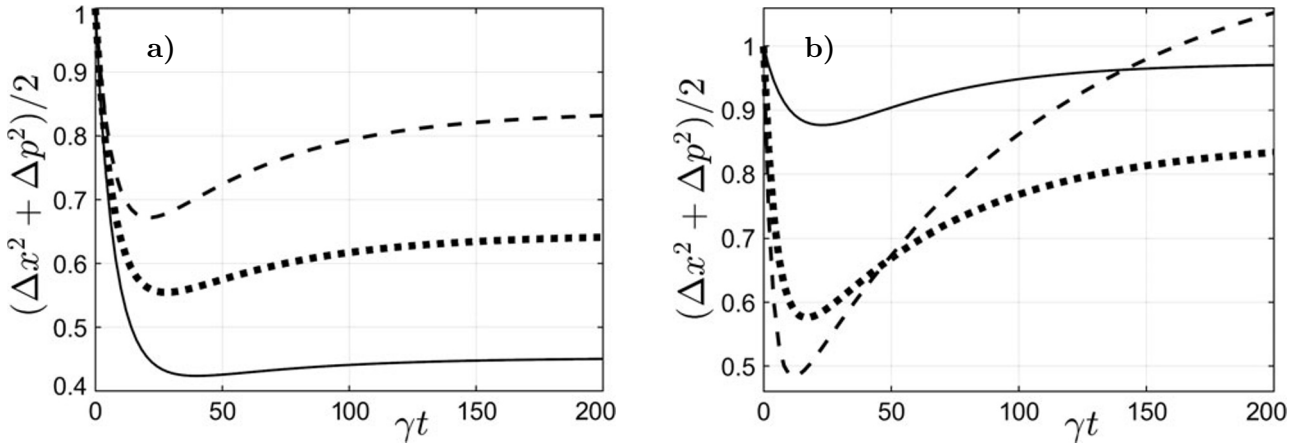

Fig. 7. Time evolution of quantum entanglement $\dfrac{\Delta x^2 + \Delta p^2}{2}$ of the photon pairs against the dimensionless parameter γt for $r_a = 10$ kHz, $\kappa = 0.5$ kHz, $\eta = 0.1$, $g = 0.8\gamma$, $\xi = 0.1\gamma$, $\theta = 0.01$, $\bar{N}_{\rm th} = 0.00$ (the solid curve), 0.25 (the dotted curve), and 0.50 (the dashed curve) (a) and $\bar{N}_{\rm th} = 0.50$, $\kappa = 0.5$ kHz, $\eta = 0.1$, $g = 0.8\gamma$, $\xi = 0.1\gamma$, $\theta = 0.01$, $r_a = 5$ (the solid curve), 15 (the dotted curve), and 25 kHz (the dashed curve) (b).

In Figs. 7 and 8, we demonstrate the dynamics of quantum entanglement by alternatively varying other parameters. We show that photon pairs are initially not in the entangled state. At the early states of the dynamical processes, entanglement quickly increases with time until it achieves a certain maximum strength. After that, it slowly decreases with time. The entanglement degree obtained here and shown in Fig. 7 b at $\gamma t = 15$ is higher than the previously reported amount of entanglement under the steady-state condition. This should indicate that quantum coherence maximally couple the photon pairs before the optical system reaches a steady state condition. The maximum achievable strength of quantum entanglement enhances with increased rate of atomic injection.

Distinct from the quantum discord, quantum

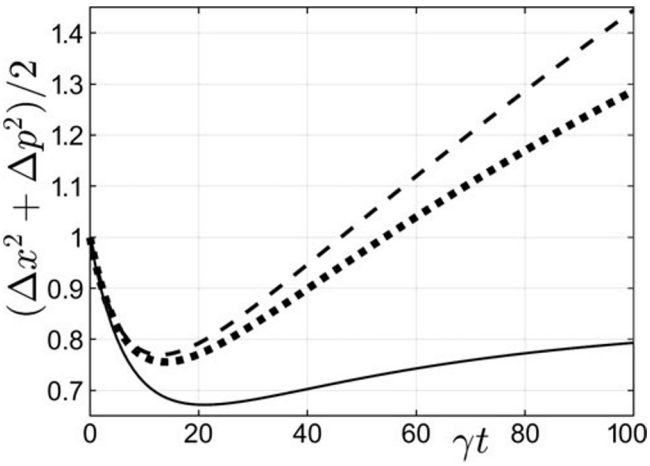

Fig. 8. Time evolution of quantum entanglement $(\Delta x^2 + \Delta p^2)/2$ of the photon pairs against the dimensionless parameter γt for $\bar{N}_{\rm th} = 0.5$, $\kappa = 0.5$ kHz, $\eta = 0.1$, $g = 0.8\gamma$, $\xi = 0.1\gamma$, and values of $\theta = 0.00$ (the solid curve), 0.0125 (the dashed curve), 0.015 (the dotted curve), at $r_a = 5$ kHz.

entanglement wipes out with increased decoherence originated from the heat-bath temperature and atomic phase fluctuations; see Figs. 7 b and 8. The influence of the quantum decoherence increases as time passes by. In the long time scale, quantum decoherence would get a chance to increase their impacts, by instigating other factors within the system. In such a case, the quantum coherence will become smaller competitive and finally fade away.

3.3. Quantum Discord

In classical system, it is possible to obtain all information on the system without disturbing it. However, this is not the case in quantum mechanics, since measurements can, in general, modify quantum systems. Owing to this fact, the two equivalent expressions of mutual information in classical information theory are not the same for quantum systems. The difference between these equivalent quantities is used to define quantum discord $D^{\hat{o}_1}$, which is a quantum correlation beyond entanglement and is given by

$$D^{\hat{o}_1} = I(\hat{\rho}) - \max_{\Pi_B^j}[J(\hat{\rho})], \tag{42}$$

where $\hat{\rho} = \rho(\hat{o}_1, \hat{o}_2)$ represents the density operator of the combined system, and

$$I(\hat{\rho}) = S(\hat{o}_1) + S(\hat{o}_2) - S(\hat{\rho}) \tag{43}$$

is the quantum mutual information that provides a measure of the total correlations within a bipartite system. In this descriptions, $S(\hat{o}_1)$ and $S(\hat{o}_2)$ represent the von Neumann entropy of each modes, while $S(\hat{\rho})$ is the joint von Neumann entropy of the bipartite system. On the other hand, $J(\hat{\rho})$ represents the classical mutual information that captures the classical correlations given by [30] $J(\hat{\rho}) = S(\hat{o}_1) - S\left(\hat{\rho}\,(\hat{o}_1, \hat{o}_2)\,\middle|\prod_{\hat{o}_2}^{j}\right)$. Here, the term $S\left(\hat{\rho}\,(\hat{o}_1, \hat{o}_2)\,\middle|\,\prod_{\hat{o}_2}^{j}\right)$ indicates that the conditional von Neumann entropy of modes $\hat{o}_1$ and $\hat{o}_2$, with $\prod_{\hat{o}_2}^{j} = |j_{\hat{o}_2}\rangle\langle j_{\hat{o}_2}|$ being a set of local projective measurements on light mode $\hat{o}_2$. An optimization condition should be imposed on $J(\hat{\rho})$ to avoid the dependence of quantum discord on the measurements [31]; this reads

$$\max_{\Pi_B^j}[J(\hat{\rho})] = S(\hat{o}_1) - \min_{\Pi_B^j}\left[S\Big(\hat{\rho}(\hat{o}_1, \hat{o}_2)\Big|\prod_{\hat{o}_2}^{j}\Big)\right]. \tag{44}$$

The optimization process of measurements of mutual information highly complicates the quantification of quantum discord in general. The continuous variable Gaussian quantum discord for two-mode radiation described by a covariance matrix G is given by [31, 32]

$$D^{\hat{o}_1} = I\left[m_{33}(t)\right] - I(s_-) - I(s_+) + I(\sqrt{\varpi}), \tag{45}$$

where

$$\varpi = \begin{cases} \dfrac{2(m_{13})^4 + [(m_{33})^2 - 1][\det(G) - (m_{11})^2] + 2|m_{13}^2|\sqrt{(m_{13})^4 + [(m_{33})^2 - 1][\det(G) - (m_{11})^2]}}{[(m_{33})^2 - 1]^2} & \text{if } c \geq 0, \\ \dfrac{(m_{11}m_{33})^2 - (m_{13})^4 + \det(G) - \sqrt{(m_{13})^8 + [\det(G) - (m_{11}m_{33})^2]^2 - 2(m_{13})^4[\det(G) + (m_{11}m_{33}]^2)}}{2(m_{33})^2} & \text{if } c < 0, \end{cases}$$

with $c = \left[(m_{11})^2 + 1\right]\left[\det(G) + (m_{33})^2\right] - \left[\det(G) - (m_{11}m_{33})^2\right]^2$. Also, we note that, for any variable x, the function $I(x)$ is defined by $I(x) = \left(\frac{1+x}{2}\right)\log_2\left(\frac{1+x}{2}\right) - \left(\frac{1-x}{2}\right)\log_2\left(\frac{1-x}{2}\right)$. In these equations, we have not shown the time dependence to save environment.

The quantum discord for the other mode $\hat{o}_2$ can be easily obtained by swapping the role of $m_{11}(t)$ and $m_{33}(t)$; this reads

$$D^{\hat{o}_2} = I(m_{11}(t)) - I(s_-) - I(s_+) + I(\sqrt{\varpi'}), \tag{46}$$

where

$$\varpi' = \begin{cases} \dfrac{2(m_{13})^4 + [(m_{11})^2 - 1][\det(G) - (m_{33})^2] + 2|m_{13}^2|\sqrt{(m_{13})^4 + [(m_{11})^2 - 1][\det(G) - (m_{33})^2]}}{[(m_{11})^2 - 1]^2} & \text{if } c \geq 0, \\ \dfrac{(m_{11}m_{33})^2 - (m_{13})^4 + \det(G) - \sqrt{(m_{13})^8 + [\det(G) - (m_{11}m_{33})^2]^2 - 2(m_{13})^4[\det(G) + (m_{11}m_{33}]^2)}}{2(m_{11})^2} & \text{if } c < 0. \end{cases}$$

In order to investigate the time evolution of the quantum discord, we plot $D^{\hat{o}_1}$ versus the dimensionless parameter γt, by alternatively varying other parameters of systems. According to the definition of quantum discord, the two-mode radiation fields are entangled for $D^{\hat{o}_1}(D^{\hat{o}_2}) > 1$, and the two-mode fields can either be in a separable or entangled states for $0 \leq D^{\hat{o}_1}(D^{\hat{o}_2}) < 1$.

In Fig. 9 a, we demonstrate the time evolution of quantum discord associated to the individual light modes. It is common knowledge that quantum discord is an asymmetric quantum correlation; this point is clearly indicated in the figure, especially in the long time scale. However, significant difference between $D^{\hat{o}_1}$ and $D^{\hat{o}_2}$ is not observed for $\gamma t = [0, 20]$, and the general profile of both curves follows the same dynamical behavior. After passing the overlapping point around $\gamma t = 20$, at which $D^{\hat{o}_1}$ starts deviating from $D^{\hat{o}_2}$, we observe that mode $\hat{o}_1$ captures stronger quantum correlation than mode $\hat{o}_1$, since $D^{\hat{o}_1} > D^{\hat{o}_2} > 1$. This result is in line with the definition of the continuous-variable quantum discord, one of the quantifiers of quantum correlations. The fact that both $D^{\hat{o}_1}$ and $D^{\hat{o}_2}$ demonstrate the same dynamical behavior and the former is stronger than the latter provides the possibility to use $D^{\hat{o}_1}$ for making sufficient analysis of quantum discord generated in the quantum system.

In Fig. 9 b, we demonstrate the time evolution of the continuous-variable Gaussian quantum discord $D^{\hat{o}_1}$ under different system parameters. We see that $D^{\hat{o}_1}$ vanishes at $t = 0$, and later $D^{\hat{o}_1}$ quickly

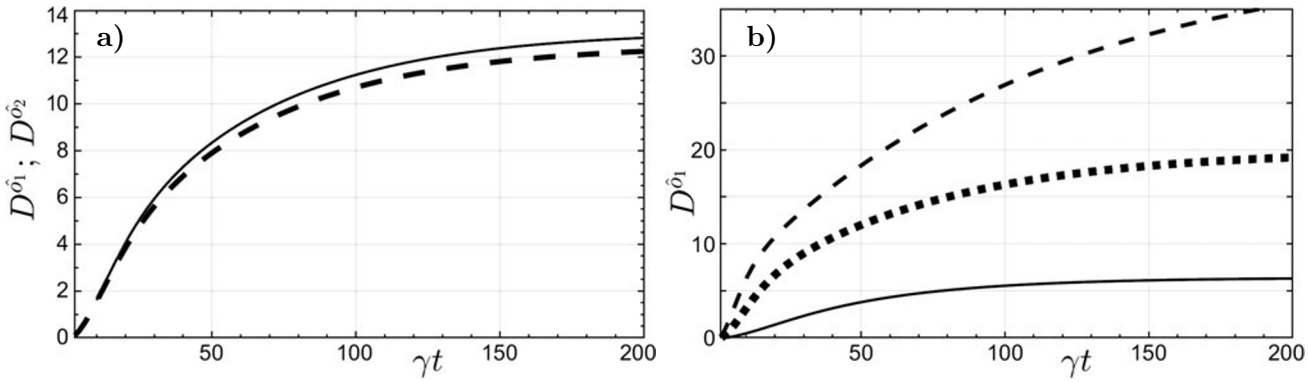

Fig. 9. Time evolution of quantum discord $D^{\hat{o}_1}$ (the solid curve) and $D^{\hat{o}_2}$ (the dashed curve) for $\bar{N}_{\rm th} = 0.5$, $\kappa = 0.5$ kHz, $\eta = 0.1$, $g = 0.8\gamma$, $\xi = 0.1\gamma$, $\theta = 0.00$, and $r_a = 10$ kHz (a) and $D^{\hat{o}_1}$ for $\bar{N}_{\rm th} = 0.5$, $\kappa = 0.5$ kHz, $\eta = 0.1$, $g = 0.8\gamma$, $\xi = 0.1\gamma$, $\theta = 0.00$, and $r_a = 5$ (the solid curve), 15 (the dotted curve), and 25 kHz (the dashed curve) (b).

increases for a short time scale and slowly increases, when the effect of the other system parameters begins to contribute to the dynamical behavior. This clearly shows absence of quantum discord and entanglement-based correlations in the system at the initial stage of system dynamics. In later stages of the process, light matter interaction can take place within the cavity mirrors to initiate fast generation of strongly coupled photon pairs, which is a resource for the observed quantum discord. Moreover, increase in the considered system parameters improves the strength quantum discord.

4. Conclusions

In this work, we studied in details the survival and sudden death of quantum correlations in an open atomic laser system, using the master equation in the good-cavity limit with the linear and adiabatic approximations. We calculated the temporal evolution of the first and second moments of the cavity mode variables, using the master equation; different amounts of interest were attained with the aid of these findings. Quantum coherence in the system were induced by a coherent inducing classical field and atomic state superpositions, and their strength was tested in the face of quantum decoherence, due to heat-bath temperatures and atomic phase fluctuations. We studied the dynamics of quantum correlations, using the standard master equation and considering different working conditions. Using various system parameters, including the atomic injection rate and the quantum coherence that arise when atoms in the laser system interact with photon pairs on sufficient time scales, and with near-maximum atomic state superpositions $\eta = 0.1$, a significant amount of quantum correlation was generated. In particular, quantum steering vanishes in the regime of strong coupling, where remarkable quantum discord and entanglement are observed for the same system parameters. This is due to the fact that the classical field is efficiently used to induce quantum coherence, only when there is a sufficient number of atoms in the excited energy state, while pumping atoms from the ground state to the excited state would be an additional task for the field, if none of them is initially in the excited state. In contrast to quantum discord, which increases with quantum decoherence, quantum entanglement and quantum steering disappear with increasing decoherence, due to the temperature of the heat bath and atomic phase fluctuations. The strength of quantum steering is maintained over a long period of time in the presence of thermal decoherence, but decreases slightly with time in the presence of phase fluctuations. However, the peaks of quantum entanglement are short-lived and suffer sudden death on the long time scale due to quantum decoherence.

Generally, we observed that the quantum correlations in the atomic laser system were strong and well preserved. However, as time progressed, the open nature of the system led to the gradual decay of these correlations. Environmental noise and interactions with the surrounding environment were identified as major factors contributing to this decay. Surprisingly, the study also revealed the occurrence of sudden death of quantum correlations under specific conditions. We found that, after a certain time, the correlations could vanish abruptly, resulting in a complete loss of quantum coherence in the system. This sudden death phenomenon has significant implications for the preservation and manipulation of quantum information in practical applications.

Acknowledgments

The authors acknowledge support from Jimma University, College of Natural Sciences, Research and Postgraduate Coordinating Office through a Mega Project Grant No. CNS-PHYS-14-2022/21.

References

1. B. Zygelman, *A First Introduction to Quantum Computing and Information*, Springer International Publishing, USA (2000).
2. C. H. Bennett and D. P. DiVincenzo, *Nature*, **404**, 247 255 (2000).
3. G. Benenti, G. Casati, D. Rossini, and G. Strini, *Principles of Quantum Computation and Information*, World Scientific Publishing Co., Singapore (2019).
4. A. Streltsov, G. Adesso, and M. B. Plenio, *Rev. Mod. Phys.*, **89**, 041003 (2017).
5. E. Mosisa, *Adv. Math. Phys.*, **2021**, 1 (2021); DOI: 10.1155/2021/6625690
6. M. Erhard, M. Krenn, and A. Zeilinger, *Nat. Rev. Phys.*, **2**, 365 (2020).
7. F. Shahandeh, A. P. Lund, and T. C. Ralph, *Phys. Rev. A*, **99**, 052303 (2019).
8. M. Cuzminschi and A. Isar, *Romanian J. Phys.*, **66**, 112 (2021).
9. B. Deveaud, A. Quattropani, and P. Schwendimann, *Quantum Coherence in Solid State Systems*, UK, IOS Press (2009).
10. Z. Alessandro, J. Fiurášek, and M. Bellini, *Nat. Photonics*, **5**, 52 (2011).
11. X. Zhan, *Phys. Rev. A*, **103**, 032437 (2021).
12. T. Yoshiaki, M. Tanaka, N. Iwasaki, et al., *Sci. Rep.*, **8**, 1 (2018).
13. O. Kfir, *Phys. Rev. Lett.*, **123**, 103602 (2019).
14. E. Darsheshdar, M. Hugbart, R. Bachelard, and C. J. Villas-Boas, *Phys. Rev. A*, **103**, 053702 (2021).
15. S. Mahmoodian, M. Cepulkovskis, S. Das, et al., *Phys. Rev. Lett.*, **121**, 143601 (2018).
16. C. Gashu and T. Abebe, *Phys. Scr.*, **95**, 075105 (2020).
17. G. K. Kitaeva, A. A. Leontyev, and P. A. Prudkovskii, *Phys. Rev. A*, **101**, 053810 (2020).
18. V. N. Chernega and O. V. Man'ko, *J. Russ. Laser Res.*, **41**, 1 (2020).
19. S. Tesfa, *Quantum Optical Processes: From Basics to Applications*, Springer Nature, USA (2020).
20. C. G. Feyisa, T. Abebe, T. Tessema, et al., *J. Russ. Laser Res.*, **42**, 1 (2021).
21. S. Ullah, H. S. Qureshi, and F. Ghafoor, *Opt. Express*, **27**, 26858 (2019).
22. W. H. Louisell, *Quantum Statistical Properties of Radiation*, Wiley, New York (1973).
23. E. A. Sete, *Phys. Rev. A*, **84**, 063808 (2011).
24. S. Tesfa, *Phys. Rev. A*, **83**, 023809 (2011).
25. S. M. Barnett and P. M. Badmore, *Methods in Theoretical Quantum Optics*, Oxford University Press, New York (1997).
26. G. S. Agarwal, "Quantum Statistical Theories of Spontaneous Emission and their Relation to other Approaches," in: G. Höhler (Ed.) *Quantum Optics. Springer Tracts in Modern Physics, vol. 70*, Springer, Berlin, Heidelberg (1974); DOI: 10.1007/BFb0042382
27. Q. Y. He, Q. H. Gong, and M. D. Reid, *Phys. Rev. Lett.*, **114**, 060402 (2015).
28. I. Kogias, R. A. Lee, S. Ragy, and G. Adesso, *Phys. Rev. Lett.*, **114**, 060403 (2015).
29. L. M. Duan, G. Giedke, J. I. Cirac, and P. Zoller, *Phys. Rev. Lett.*, **84**, 4002 (2000).
30. K. Umemoto, *Phys. Rev. D*, **100**, 126021 (2019).
31. G. Adesso and A. Datta, *Phys. Rev. Lett.*, **105**, 030501 (2010).
32. J. S. Zhang and Ai-Xi Chen, *Quantum Phys. Lett.*, **1**, 69 (2012).